Experimental and Numerical Investigations of Flow Characteristics Over Half Sphere Positioned at Unfavorable Angle to The Flow

M. Bassam Wafa Nabhan
Department of Mechanical Engineering
College of Engineering, University of Bahrain
Isa Town, Kingdom of Bahrain

***Abstract*-- The airflow characteristic over the smooth wall surface of a heated and tilted hemisphere immersed in a fully developed flow in a test wind tunnel is investigated experimentally and numerically. K-type thermocouples are used to analyze the flow structure for different regions of flow domain around the front and back surfaces of the hemisphere. The investigation is carried at air velocity of 25 m/s with corresponding Reynolds number of $2.5E^{+05}$. The total drag over the hemisphere is experimentally measured in the sub-sonic wind tunnel with electronic balance sensors at the test flow velocity. Corresponding numerical simulations using Fluent software code are also carried out to visualize the flow reversal, separation, horseshoe vortices, and recirculation zone downstream and back of the hemisphere and to validate the experimental results. The heat transfer enhancement exemplified by local Nusselt and Reynolds number on the hemisphere surface is also studied. It is shown that the flow characteristics vary on the stream-wise and back surfaces as the flow becomes unsteady.**

***Index Term*-- flow over isothermal hemisphere, forced convection, CFD simulation, heat transfer enhancement.**

I. INTRODUCTION

The aerodynamic characteristics of a bluff body immersed in a turbulent boundary layer have attracted the attention of many investigators in the field of industrial aerodynamics. Most of the previous studies have concerned two-dimensional bluff bodies, such as normal plates [1-4], inclined plates [5], and semicircular cylinders [6]. The curved shape of a hemisphere structure makes the accurate estimation of the air pressure a difficult task due to Reynolds number effects. Several research papers have focused on this subject. Maher [7] reported that the Reynolds number becomes invariant when Reynolds number exceeds $1.4E^{+06}$. In addition Taylor [8] suggests that, when Reynolds number exceeds $2E^{+05}$ and turbulence intensity exceeds 4%, the pressure distribution becomes Reynolds number independent. Ogawa [9] indicates that for Reynolds numbers ranging from $1.2E^{+05}$ to $2.1E^{+05}$, level of turbulence has little effect upon the mean pressure distribution. Toy and Moss [10] have shown that, with increase of turbulence intensity, separation region and reattachment point move downstream.

Moreover, forced convection heat transfer from isothermal or isoflux external bluff surfaces is an important problem for aeronautic engineers. There are many engineering systems that are modeled using forced convection, such as electronic components on printed circuit boards placed in cabinets, hot-wire anemometers, transformers, heat sinks, thermal spreaders, and heat exchanger design. Several researchers have investigated forced convection from isothermal axi-symmetric bluff bodies, such as spheroids (Beg [11]), cylinders (Refai and Yovanovich [12]), and discs (Wedekind and Kobus [13]) using a variety of predictive methods as reviewed in (Yovanovich [14]). However, the number of studies from steady laminar and turbulent forced convection is limited on hemispherical bluff bodies, with most research restricted to experimental studies (Igarashi [15, 16]) leading to empirical correlations or detailed numerical procedures (Wong and Chen [17]).

The objective of this paper is to investigate air flow characteristics around a heated isothermal surface of a hemispherical body tilted at 52 degrees to the free stream air flow direction. Having the flow field, local pressure and heat flux distribution, recirculation zones, flow separation region, and reattachment locations will be investigated at $Re = 2.5E^{+05}$ using experimental measurements and numerical simulation.

II. EXPERIMENTAL WORK

Experimental investigations are performed in a sub-sonic wind tunnel located in the Fluids Laboratory in the Mechanical Engineering Department at Bahrain University. The tunnel cross section is a transparent 150 mm square working section with an overall length of 450 mm. Air is drawn in through a variable speed fan located at the discharge end of the tunnel to minimize turbulence inside the working section. A honeycomb type flow straightener and 9.4:1 contraction ratio ensure well developed air flow through the working section. An Electronic Balance and software, allows full electronic monitoring and recording of the measured drag and lift on the software mimic diagram of a suitable PC. The model being tested can be rotated on the mounting and the angle of rotation measured electronically. The operating range is nominally 0 – 32 m/s with no model installed in the working section. The maximum

velocity achievable in the test section varies with the model type and the blockage created by the model. The air velocity is adjusted from the software by altering the fan speed. Fan speed is set as a percentage of the maximum speed, between 0% and 100%. The corresponding static head in the tunnel given as the differential head between the tunnel and atmosphere and air velocity in m/s are displayed on the software mimic diagram.

The experimental setup consists of a smooth suspended hemisphere in the test section tilted at 52 degrees to the vertical y-direction. The location of the model in the test tunnel and the reference coordinate system are shown in FIG.1.The experimental setup consists of a smooth immersed hemisphere of diameter 6.5 cm in the test section of the wind-tunnel. To avoid wall interference, the model is supported from the rear with an aluminium rod of 0.05D, where D is the diameter of the hemisphere. In addition, the tunnel blockage was overcome by reducing the Mach number value to below 0.1 as stipulated by Naumann (1953) (E. Achenback [18]). At, for instance, the maximum Reynolds number, which was obtained in the tunnel test section, the Ma number was even lower than 0.05.

A filament heater attached to an external power supply and embedded inside the hollow cavity of the hemisphere is used to raise the hemisphere surface temperature isothermally to 70 ^{O}C. A total of fifteen (15) K-type thermocouples are embedded in the front and back surfaces of the hemisphere and attached to a digital temperature recorder to detect the temperature readings at 25 m/s and various test air flow velocity. The temperature readings are taken in the stream-wise and back surfaces of the hemisphere as shown in FIG. 2.

III. RESULTS

The flow characteristics of the 52^{o} tilted model hemisphere are determined at the test air flow velocity. The total drag force is measured using an Electronic Balance of the wind tunnel and software on a mimic diagram of a suitable PC. The measurements were taken for cold model temperature of 20 ^{o}C and hot isothermal temperature of 70 ^{o}C. These results are shown in FIG.3. The total drag coefficient, Cd at the mean test velocity in the duct is calculated using the relationship;

$$Cd = \frac{\Sigma DT}{0.5\,\rho\, V^2 A \sin\alpha} \qquad (1$$

The results of drag coefficient, Cd for cold and hot conditions are plotted against Reynolds numbers, Re as shown in FIG.3. In the cold condition the drag coefficient increases with Re up to Re = 1.5E^{05} and stays almost constant for larger Re values. Perhaps, this is a result of turbulent flow, boundary layer separation and reverse flow due to adverse pressure gradient and large pressure drag taking place at the same point on the upper surface of the hemisphere. Similar trend, however with larger values of Cd are noted for the hot hemisphere with invariant Cd values at Re = 2E^{+05} and above. This perhaps is attributed to the larger boundary layer thickness for the heated hemisphere surface. As a result, Cd is affected by many factors namely; the fluid viscosityμ, the flow velocity gradient $(\partial u/\partial y)_s$, and the thermal boundary layer temperature gradient $(\partial T/\partial y)_s$. An increase on the surface temperature will give rise to larger values of μ and a decrease in $(\partial u/\partial y)_s$ due to buoyancy effect for a mixed convection mode. Perhaps the increase in the viscosity is predominant factor in the drag equation. And thus the skin friction drag increases on the surface leading to larger total drag in comparison to the hemisphere surface cold condition. The total drag coefficient Cd for the inclined hemisphere can be written in the following form;

$$C_d = \frac{\Sigma(\Delta P + \tau)}{\frac{1}{2}\rho V^2 A \sin\alpha} = \frac{\Sigma(\Delta P + \mu\frac{\partial u}{\partial y})}{\frac{1}{2}\rho V^2 A \sin\alpha} \qquad (2$$

The temperature distributions on the stream-wise and back cover of the hemisphere were measured at approximately equal locations using 15 K-type thermocouples connected to a digital temperature recorder. The temperature readings are taken at various air stream velocities, namely 5, 10, 15, 20, and 25 m/s with corresponding Reynolds numbers of 5E^{+04}, 1E^{+05}, 1.5E^{+05}, 2E^{+05}, and 2.5E^{+05}. The thermocouple locations are shown in FIG.2 (a),and (b).The temperature readings are made dimensionless ($\Delta T/T_{atm}$) with respect to the hemisphere isothermal temperature T_s, of 70 ^{o}C and the wind tunnel temperature T_{atm}, of 20 ^{o}C.

FIG.4 shows the stream-wise temperature variations on the front hemisphere surface at increasing air flow velocities of 5, 10, 15, 20, and 25 m/s with corresponding Reynolds numbers of 5E^{+04}, 1E^{+05}, 1.5E^{+05}, 2E^{+05}, and 2.5E^{+05}. It is noticed that the temperature variations ΔT increases at larger Re values.

This can be explained, as Re increases the dissipation of kinetic

energy on the surface increases.

At each Re value the temperature variation on the surface boundary of the hemisphere also changes. The boundary layer separation and reverse flow takes place due to a strong pressure gradient in the vicinity of the trailing front surface of the hemisphere at point 6 as illustrated in FIG.2 (a), where the velocity gradient $(\partial u/\partial y)_s \approx 0$ and ΔT is small due to low velocity magnitude , large boundary layer thickness and thus lower cooling effect on the surface ($\Delta T = Ts - T_{thermocouple}$). However on the leading edge of the front surface of the hemisphere, at point 1 of FIG.2 (a), the flow doesn't separate giving higher variations in ΔT due to effective cooling of the thermocouple tips as a result of thin boundary layer and strong flow momentum. At the stagnation point 3, ΔT is at its lowest value as shown.

Similar temperature variations trend is shown in FIG.5 on the back end cover. The lowest variation in ΔT takes place at Re = 5E^{+04} and increases at larger Re values. At point 17, near the center of the hemisphere back plate, ΔT is at its lowest values for all Re values, perhaps due to lowest air flow velocity in this vicinity of the flow domain. The temperature variation increases from point 16 to 14 due to increased flow recirculation in this region. ΔT remains almost invariable towards the trailing edge from point 18 to 21. It is also noted in this graph and by comparison with the stream-wise temperature variation values; the rear surface of the hemisphere is also effective in enhancing the heat transfer mode.

IV. NUMERICAL RESULTS

Numerical simulation is performed using a discretized 2-dimensional Fluent code to study the flow field, pressure distribution, and heat transfer around an immersed mounted hemisphere in more detail; the numerical simulation is related to the experimental investigations performed on the tilted hemisphere in a sub-sonic wind tunnel at 52^o to the vertical as shown in the schematic diagram in FIG.1. The origin of the coordinate system is located in the center of the hemisphere. Measured in units of the reference length of the flow problem (D is the diameter of the hemisphere), the dimensions of the computational domain are (x, y, z) = (0.15, 0.15, 0.45), and for the results presented we used a computational configuration that contained some 54787 cells, 112743 faces and 57956 nodes distributed over 6 face zones. Velocity inlet and pressure outlet were specified at the inflow and outflow boundaries, while top and bottom boundaries of the computational domain and the hemisphere front and back surfaces as wall. The inflow boundary conditions were chosen to match the velocity and turbulence profiles measured during the wind tunnel experiments. Outflow boundary conditions were chosen to maintain constant longitudinal rate of change of all dependent variables (constant slope). The governing equations of incompressible turbulent 2-D flow are solved using finite volume discretization method. To solve these equations numerically, SIMPLE algorithm which treats the coupling between velocity and pressure in the flow field is employed. Control volume cells for velocity components are staggered with respect to the main control volume cells. The Realizable κ - ε Turbulence model, which provides superior performance for flows involving boundary layers under strong adverse pressure gradients, separation, and recirculation, is used to study the numerical computation of the turbulent flow field around the hemisphere. The hemisphere is mounted on a hanger and its distance from the inlet plane in the computational domain is about 3.5 D. Non-uniform structured grid is used to discretize the governing equations. FIG.6 shows the grid generated for the numerical simulation. Finer grids are used adjacent to the obstacle where the velocity gradients are large and the recirculation is expected to develop in these regions. The grid spacing is large far from the hemisphere where the flow is without any considerable variation.

The numerical simulations were used to determine heat transfer and fluid flow in the region surrounding an isothermal hemisphere. The obstacle was modeled using four isothermal, no slip planes in contact with the fluid regions for the stream-wise, back, and top and bottom surfaces. A uniform inlet velocity U_∞ and uniform free stream temperature T_{atm} were applied at the upstream domain boundary, T_{atm} and atmospheric (zero) pressure at the downstream boundary and T_{atm} at the top and bottom wall boundaries. The hemisphere and ambient air temperature were set to T_s = 70 ^oC and T_{atm} = 20 ^oC respectively, and all air flow properties were evaluated at a mean film temperature of 318 K. In each of the CFD simulations, the tilt angle of the obstacle was kept constant at 52^o to the vertical. Numerical solution is simulated for Re = $2.5E^{+05}$. Converged solution is obtained where the values of residuals were less than 10^{-6}.

FIG.7 shows the mean centerline pressure coefficient, Cp distribution plotted versus the stream wise direction on the smooth tilted hemisphere at Re = $2.5E^{+05}$. The numerical simulations display negative pressure coefficients over the downwind face of the obstacle up to 15^o angle (67^o from vertical). Above this angle, the pressure coefficients indicate positive values up to 80^o angle. Afterwards, the pressure coefficient displays again negative values over the upwind face of the hemisphere from 80^o to 180^o angle. The negative pressures gradually recover and reach a stable value at about 150^o which indicates the point of separation on the trailing edge and beginning of the wake region. The separation point can also be observed in the velocity contour plot in FIG.8, the snap shot photo in FIG.9, and the shear stress plot in Fig.10. Moreover, in FIG.10, the multi-peaks phenomenon depicted at the beginning of the wake region at $\theta \approx 150^o$ in the trailing edge suggests that transition of separated free shear layer occurred and that a separation bubble is formed at this stage, the first and second peaks indicate the locations of fore-separation and the reattachment/rear-separation. With increasing Reynolds number the magnitude of the peak suction continuously increases whilst, the wake suction and hence the overall drag coefficient decrease. Numerically computed drag coefficients are 0.9, 1.45 and 2.33 at Re = $5E^{+04}$, $1.5E^{+05}$ and $2.5E^{+05}$ respectively. Experimentally measured values of drag coefficient for the isothermally heated obstacle at these Re values are approximately; 0.4, 0.9 and 1. The differences noted are most likely due to the quality of the free stream and three dimensional effects (vortex shedding, etc.). There are several problems with our simulation: we are modeling a steady flow, even though the actual physical flow is unsteady; and we are using a turbulence model instead of resolving all the small eddies of the turbulent flow. Another significant source of error in our calculations is that the CFD code is run with turbulence turned on in order to reasonably model the wake region, which is turbulent; however the boundary layer on the surface of the hemisphere is still laminar. The predicted location of the separation point downstream of the top of the obstacle is more in line with turbulent boundary layer separation, which does not occur until much higher values of Reynolds number. The bottom line is that CFD codes have a hard time in the transitional regime between laminar and turbulent flow, and when there is a mixture of laminar and turbulent flow in the same computational domain. In fact, most commercial CFD codes give the user a choice between laminar and turbulent - there is no "middle ground." In the present calculations, we model the boundary layer as turbulent, even though the physical boundary layer is a mixed flow; it is not surprising, then, that the results of our calculations do not agree well with experiment. If we would have instead specified laminar flow over the entire computational domain, the CFD results would have been even worse (less physical). The maximum negative value of the pressure coefficient is noted at the hemisphere leading edge, where the flow velocity and shear stress are maximum, and the maximum positive value of Cp is observed

approximately at θ = 45° (stagnation point) as depicted in FIG.7, the shear stress x-y plot in FIG. 10 and the velocity profile contour plot at Re = 2.5 E^{+05} shown in FIG.8. Cp is minimum at the point of separation θ ≈ 150°.

The effectiveness of the experimental results to predict the rate of heat transfer from an isothermally heated hemisphere tilted at 52° to the vertical is assessed through comparison with numerical predictions using the finite volume model explained earlier. The heat transfer rate is calculated at Re = $2.5E^{+05}$, where Re is based on the approach velocity, the characteristics length and the kinematic viscosity at the free stream air temperature in the test section. The hemisphere and the ambient air temperature were set at Ts = 70° and T_{atm} = 20°, and all properties were evaluated at a film temperature of 318 K. As the turbulent boundary layer grows in thickness on the surface of the obstacle, the local rate of heat transfer Q_x and thus the local heat transfer coefficient, h_x will decrease. This relation can be expressed mathematically as;

$$Q_x = h_x (T_s - T_{atm}) \quad (3)$$

$$Nu_x = \frac{hx\ x}{k} = \left\{\frac{Qx}{Ts-Tatm}\right\} \frac{x}{k} \quad (4)$$

The local Reynolds Number is defined at each x location by;

$$Re_{(x)} = Re\ (x) \quad (5)$$

In polar coordinates;

$$Nu(\theta) = \left\{\frac{Q\theta}{Ts-Tatm}\right\} \frac{D\ Sin\ (\theta + 52)}{2\ k} \quad (6)$$

$$Re(\theta) = Re\ (D/2)\ Sin\ (\theta + 52^o) \quad (7)$$

The surface heat flux is calculated at each x-location using the CFD code. The x-location is converted into angular position, θ around the hemisphere front surface. The local Nusselt number $Nu_{(\theta)}$ and Reynolds number $Re_{(\theta)}$ are computed at each angular position (θ) on the hemisphere front surface and linear location (x) on the hemisphere back surface for each wind tunnel test velocity. FIG.11 shows $Nu_{(\theta)}$ versus $Re_{(\theta)}$ plot at Reynolds number, $2.5E^{+05}$ on the front stream-wise direction. A polynomial best fit trend line of order 6^{th} is plotted to show behavior of the local heat transfer rate along the front surface. It is observed that heat transfer rate is largest on the leading edge, θ ≈ 0.13° ($Re_{(\theta)}$ = 6440 and $Nu_{(\theta)}$ = 630.8) due to maximum velocity magnitude and large kinetic energy dissipation and decreases afterwards as the flow moves upwards to the trailing edge. At θ ≈ 127° , approximately 180° from the vertical y-angular position taken in the clock-wise direction ($Re_{(\theta)}$ = 0 and $Nu_{(\theta)}$ = 400), the rate of heat transfer starts to drop sharply until the separation point where heat transfer commences to fluctuate into low and high peaks of heat transfer due to Van Karman vortex and unsteady flow behavior. On the front stream-wise direction, the minimum value of heat transfer is observed in the separation zone at θ ≈ 149.8° ($Re_{(\theta)}$ = 3058.5 and $Nu_{(\theta)}$ = 59.85). Moreover, low values of heat transfer are noticed on the leading edge on and around the stagnation point θ ≈ 45 ± 3° ($Re_{(\theta)}$ = 8001-8102 and $Nu_{(\theta)}$ = 272-296).

FIG.12 depicts the local heat transfer rate on the back surface of the hemisphere. It is observed that heat transfer is almost zero at the center of the back surface (x, y) = (0, 0) and increases in the opposite directions reaching a maximum value just before the tips of both the leading and trailing edges at $(x, y)_{leading}$ = (-24.93, -18.96) mm where, $Re_{(x)}$ = 6250 and $Nu_{(x)}$ = 240, and $(x, y)_{trailing}$ = (24, 19) mm, where $Re_{(x)}$ = 6300 and $Nu_{(x)}$ = 140 respectively as shown. It is also noticed that the rate of heat transfer on the lower surface from the center towards the leading edge has shown higher heat transfer rate in comparison with the upper surface from the center towards the trailing edge. The above behavior is due to strong recirculation flows and larger velocity magnitudes on the leading back surface compared to the trailing surface. The polynomial trend line shown on FIG.12 indicates that the local heat transfer rate on the back surface increases with increasing $Re_{(x)}$.

V. CONCLUSIONS

The main flow structures and forced convection heat transfer rate from a tilted isothermal hemisphere immersed in air flow in a subsonic wind tunnel are determined using experimental and numerical schemes. The results presented are for Reynolds number, Re = $2.5E^{+05}$ show that:

(1) The Realizable κ - ε Turbulence model slightly overestimates the stream-wise total drag over the hemisphere to the values determined experimentally. The variations are a result of the unsteady flow behavior and 3-D effects on the obstacle, which could not be catered for in the 2-D CFD simulation.

(2) The numerical investigation has shown that maximum positive value of pressure coefficient, Cp is observed at the stagnation point, θ = 45° and minimum value at the point of separation θ ≈ 150°.

(3) The simulation has shown that the transition of separation flow occurs on the trailing surface of the hemisphere at θ ≈ 150° where the drag is minimum.

(4) The experimental work and numerical simulation have shown that the heat transfer rate is large on the front leading surface of the hemisphere. This occurred as a result of larger local flow velocity, which generates a thin boundary layer and thus more effective cooling on this zone. However on the trailing surface, the overall heat transfer is lower due to low velocity magnitude and the commencement of the separation zone at θ ≈ 150°. Similar behavior on heat transfer rate has also been noted on the back surface of the hemisphere.

(5) The tilted hemisphere configuration under study has shown that the front and back surfaces are effective in heat transfer enhancement and they can complement each other.

(6) The numerical simulation has shown that the minimum value of heat transfer is observed in the separation zone at $\theta \approx 150^o$ on the front stream-wise direction. The separation zone comprised of different minima and maxima peaks of heat transfer as a result of flow separation, recirculation and unsteady flow conditions.

(7) The effective heat transfer on the hemisphere surface can be optimized by studying flow at different inclinations and the results can be compared afterwards. Also different materials and surface finish can investigated.

ACKNOWLEDGMENT

The author wishes to acknowledge the financial support of the Deanship of Research in the University of Bahrain under research project grant no.30/2011. The author appreciates this support and the comments of the reviewers.

REFERENCES

[1] M.C. Good and P.N. Joubert, 1968, The form drag of two dimensional bluff plates immersed in a turbulent boundary layer, J. Fluid Mech., 3, pp. 547-582.

[2] K.G. Range Raju, J. Loeser and E.J. Plate, 1976, Velocity profiles and force drag for turbulent boundary layer along smooth and rough flat plates, J.Fluid Mech., pp. 383-399.

[3] I.P. Castro, and J.E. Fackrell, 1978, a note on two-dimensional fence flows, with emphasis on wall constraint, J. Ind. Aerodyn., 3, pp.21-38.

[4] H.Sakamoto, M. Moriya and M. Arie, 1975, a study on the flow around bluff bodies immersed in turbulent boundary layers, Part 1, Bull. Jpn. Soc. Mech. Eng., 18, pp. 1126-1133 (in Japanese).

[5] H.Sakamoto, M. Moriya and M. Arie, 1977, a study on the flow around bluff bodies immersed in turbulent boundary layers, Part 2, Bull. Jpn. Soc. Mech. Eng., 20, pp 71-78 (in Japanese).

[6] H.Sakamoto, M. Moriya and M. Arie, 1977, A study on the flow around bluff bodies immersed in turbulent boundary layers, Part 3, Trans. Jpn. Soc. Mech. Eng., 42, pp. 3224-3232 (in Japanese).

[7] F.J. Maher, 1965, Wind loads on basic dome shapes, J. Struct. Div. ASCE ST3, pp. 219-228.

[8] T.J. Taylor, Wind pressures on a hemispherical dome, 1991, J. Wind Eng. Ind. Aerodn. 40, pp. 199-213.

[9] T. Ogawa, M. Nakayama, S. Murayama, Y. Sasaki, 1991, Characteristics of wind pressures on basic structures with curved surfaces and their response in turbulent flow, J. Wind Eng. Ind. Aerdyn. 38, pp. 427-438.

[10] N. Toy, W.D. Moss, E. savory, 1983, Wind tunnel studies on a dome in turbulent boundary layers, J. Wind Eng. Ind. Aerdyn. 1, pp. 201-212.

[11] Beg, S.A., 1975, Forced convection mass transfer studies from spheroids, Warme-und Stoffubertragung, 8, pp. 127-135.

[12] Refai-Ahmed, G., and Yovanovich, M. M., 1970, Experimental study of forced convection from isothermal circular and square cylinders and toroids, ASME J. Heat Transfer, 119, pp. 70-79.

[13] Wedkind, G. L., and Kobus, C. J., 1996, Predicting the average heat transfer coefficient for an isothermal vertical circular disc with assisting and opposing combined forced and natural convection, Int. J. Heat Mass Transfer, 39 , No. 13, pp. 2843-2845.

[14] Yovanovich, M. M., and Vanoverbeke, C. A., 1988, Combined natural and forced convection heat transfer from isothermal spheres, paper No. 88-2618, AIAA thermo-physics, Plasama-dynamics and Lasers conference, San Antonio, TX.

[15] Igarashi, T., 1985, Heat transfer from a square prism to an air stream, Int. J. Heat Mass Transfer, 28, No.1, pp. 175-181.

[16] Igarashi, T., 1986, Local heat transfer from a square prism to an air stream, Int. J. Heat Mass Transfer, 29, No.5, pp. 774-784.

[17] Wong, K. L., and Chen, C. K., 1986, Finite element solutions for laminar flow and heat transfer around a square prism, Journal of the Chinese institute of Engineers, 9, No.7, pp. 605-615.

[18] E. Achenback, 1972, Experiments on the flow past spheres at very high Reynolds numbers, J. Fluid Mech., vol.54, part 3, pp. 565-575.

NOMENCLATURE

A	Projected surface area of hemisphere, m^2
Cd	Total drag coefficient
D_T	Total drag force, N
V	Free air stream velocity, m/s
P	Pressure, Pa
T_{atm}	Wind tunnel temperature, ^oC
T	Temperature recorded by thermocouples during tests, ^oC
T_s	Hemisphere isothermal temperature, ^oC
Re	Reynolds number in the test section
Re_x	Local Reynolds number
Q_x	Local rate of heat transfer, W
h_x	Local heat transfer coefficient, $W/m^2.K$
x	x-location on the surface of the hemisphere
θ	Angular location on stream-wise surface
ρ	Air flow density, kg/m^3
α	Hemisphere inclination with the horizontal
ΔT	$(T_s - T)\ ^oC$
μ	Air dynamic viscosity, kg/m.s
$(\partial u/\partial y)_s$	Velocity gradient on the surface, s^{-1}
$(\partial T/\partial y)_s$	Thermal boundary layer temperature gradient, $^oC/m$
τ_{wf}	Shear stress along front hemisphere surface, Pa

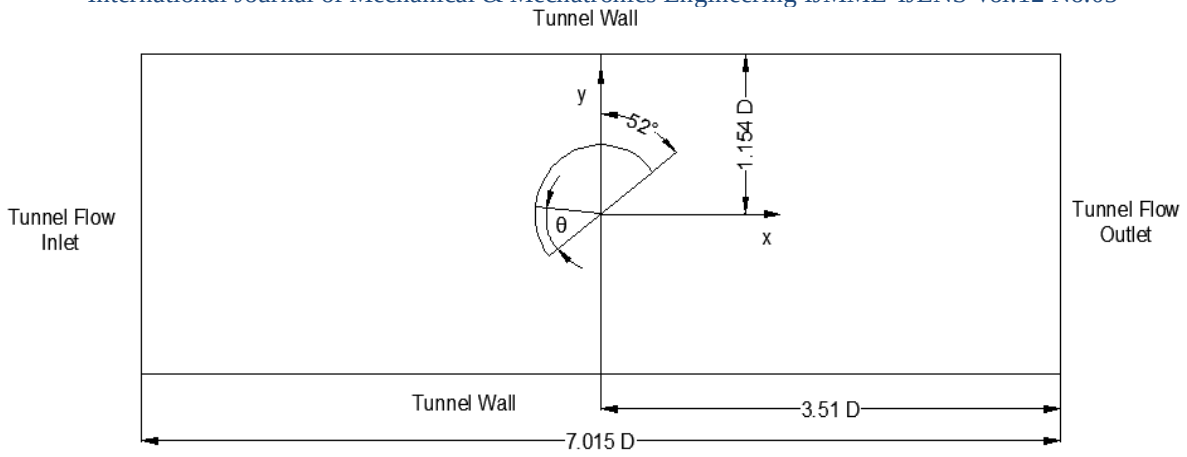

Fig. 1. Schematic of the model hemisphere in the test tunnel with reference coordinates system

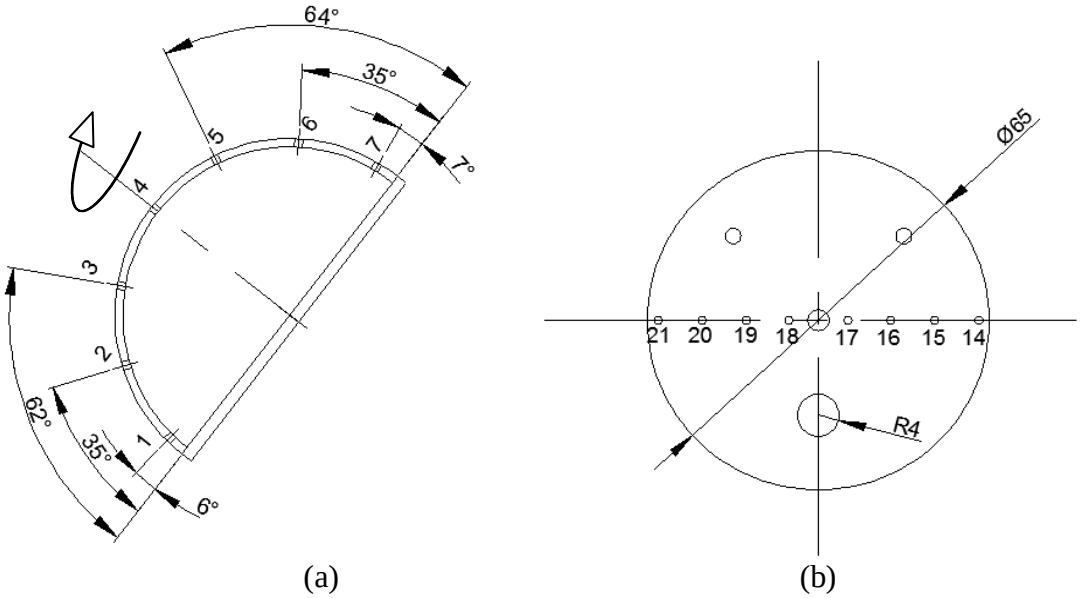

Fig. 2. Hemisphere at 52 degrees tilt angle showing thermocouple positions
(a) Thermocouples location in stream-wise direction, and (b) Back end cover

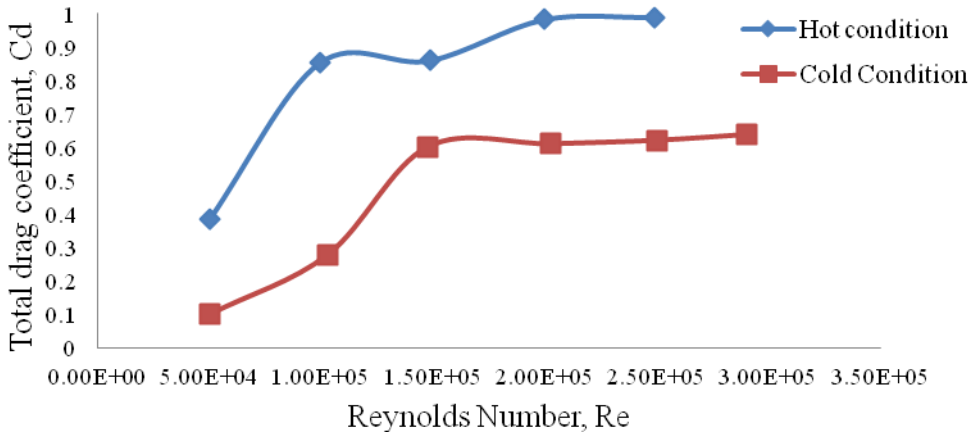

Fig. 3. Drag coefficients for hemisphere versus Reynolds number at cold and hot condition

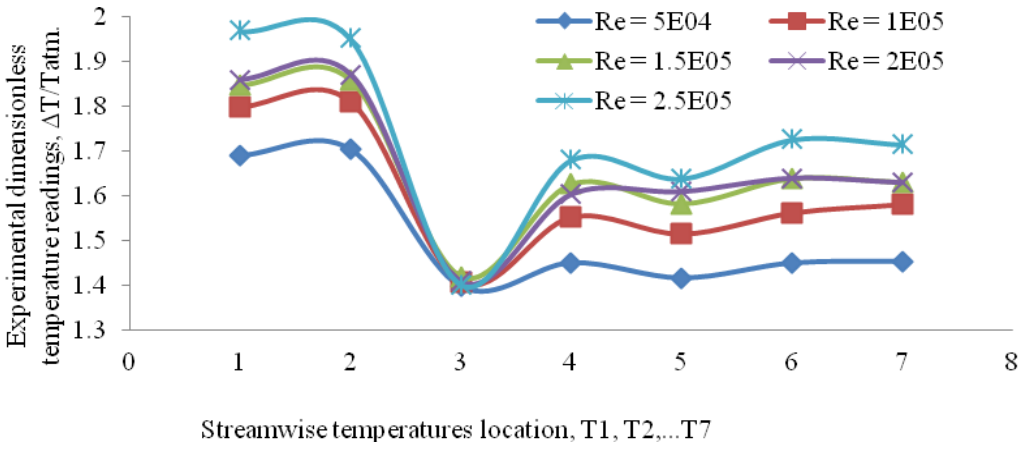

Fig. 4. Frontal hemisphere stream-wise dimensionless temperature variations at 52 deg. tilt angle

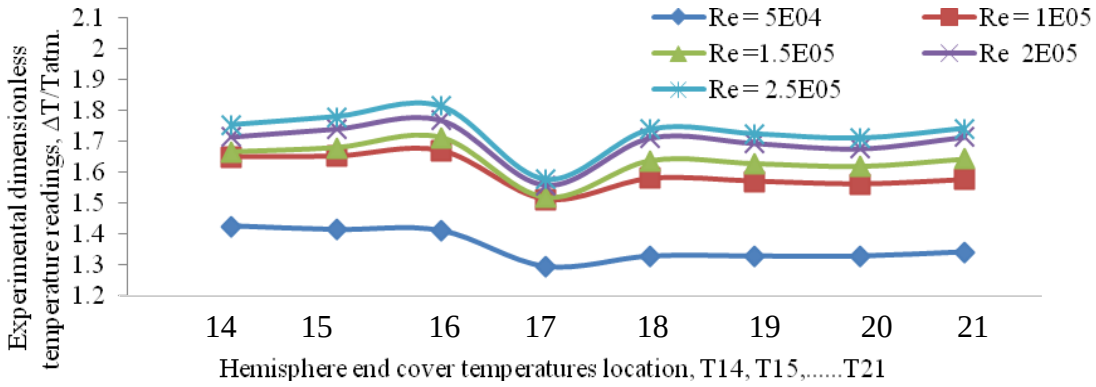

Fig. 5. Hemisphere back end dimensionless temperature variations

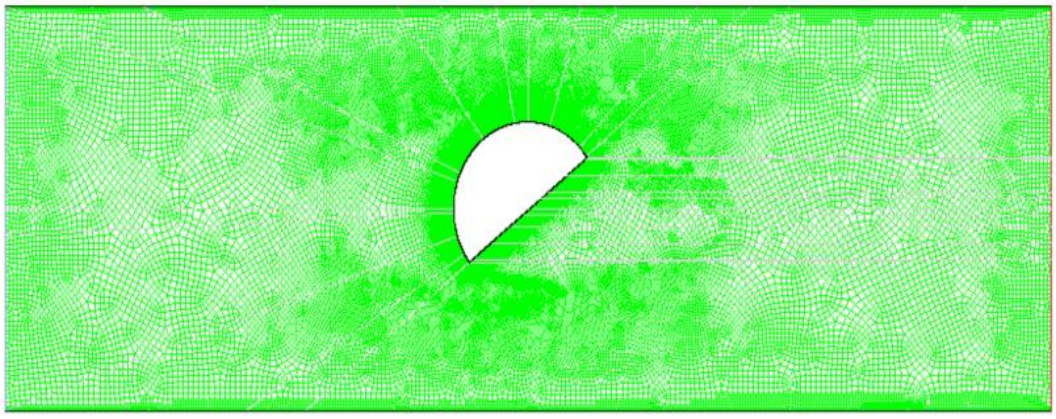

Fig. 6. Grid arrangement

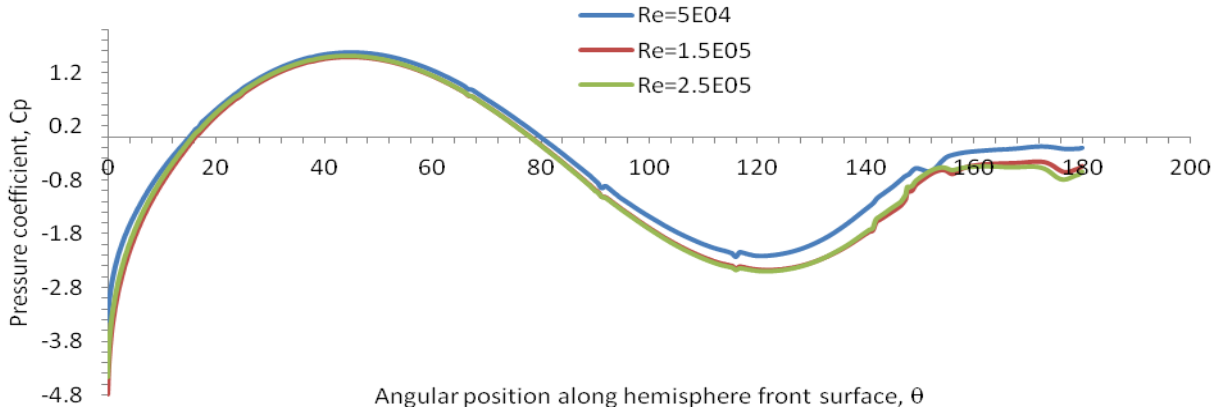

Fig. 7. Pressure Coefficient, Cp along hemisphere front surface

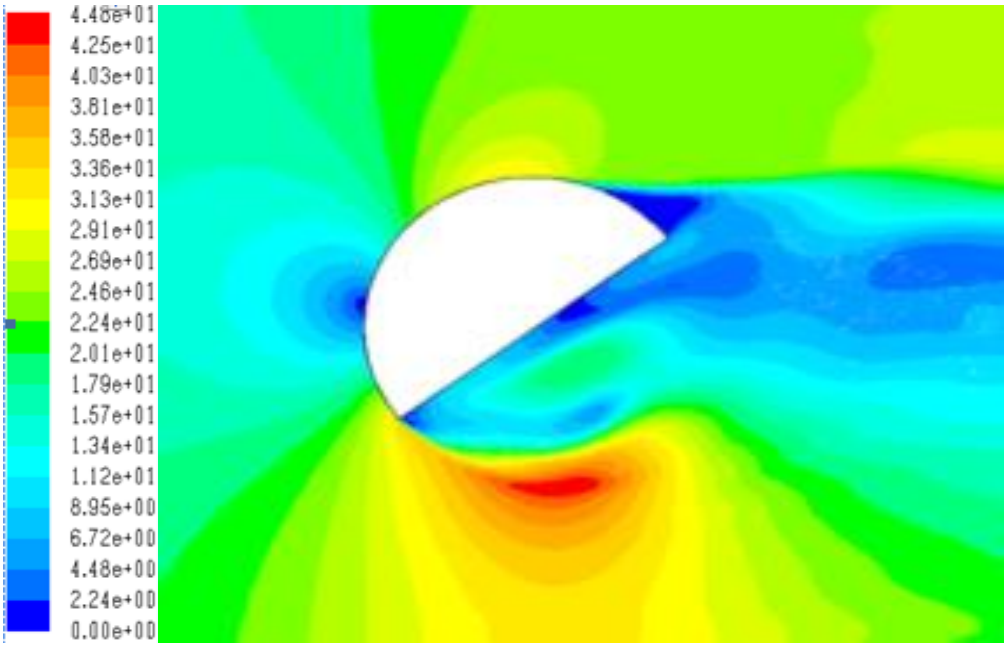

Fig. 8. Velocity magnitude contour plot at Re = 2.5 E^{+05}

Fig. 9. Smoke generated flow around hemisphere showing separation flow on the trailing surface, Re = 2.5E^{+05}

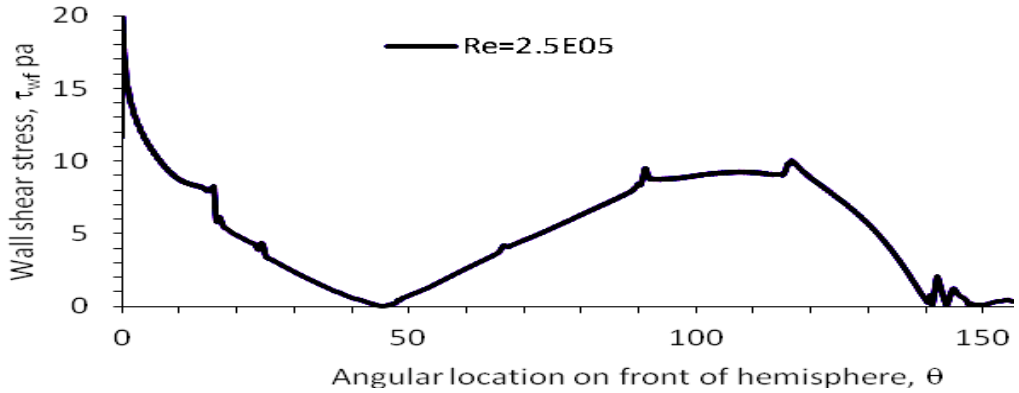

Fig. 10. Shear stress, τ_{wf} along hemisphere front surface

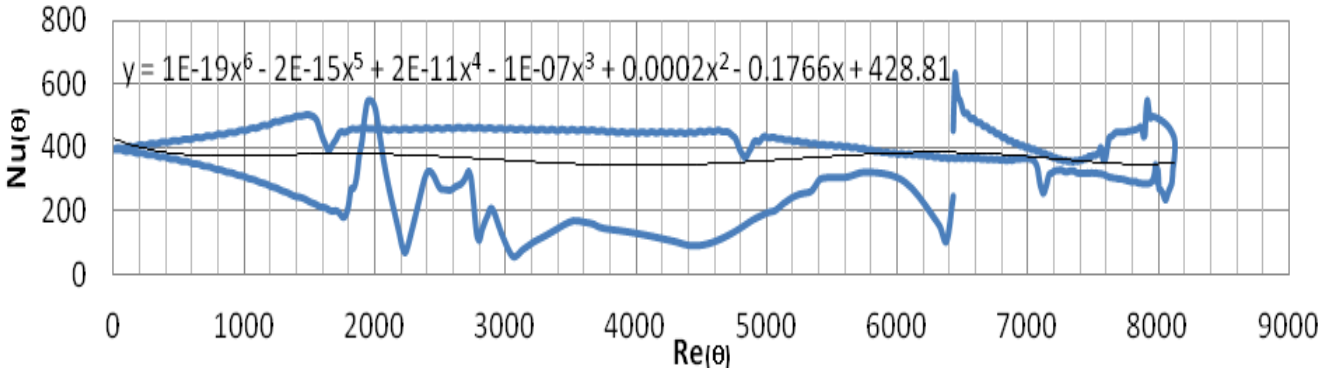

Fig. 11. Local Nusselt and Reynolds numbers on front of hemisphere, Re = $2.5E^{+05}$

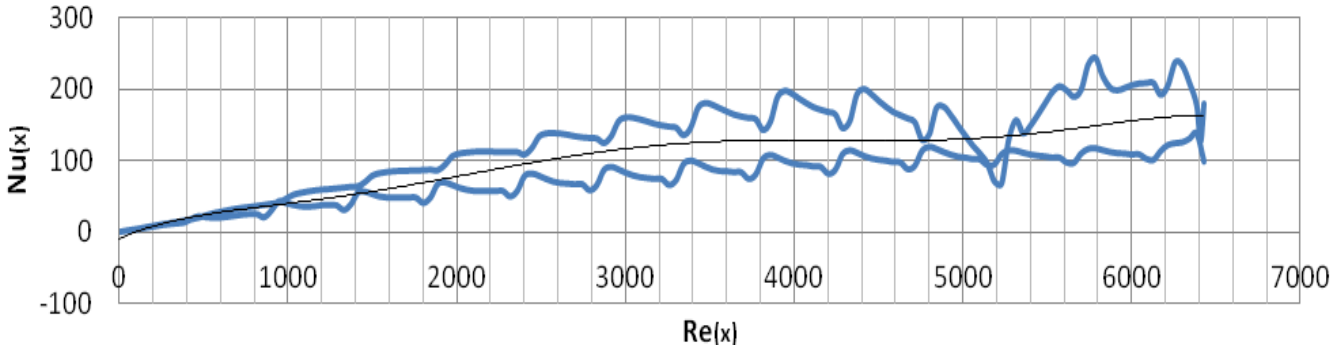

Fig. 12. Local Nusselt and Reynolds numbers on back of hemisphere, Re = $2.5E^{+05}$